Working title:

A REEVALUATION OF FACIES ON GREAT BAHAMA BANK I: New Facies Maps of Western Great Bahama Bank

John J.G. Reijmer[1,2,3] [(*)], Peter K. Swart[4], Thorsten Bauch[1,5], Robert Otto[4], Lars Reuning[1,6], Sven Roth[1,7], and Susanne Zechel[1,8]

1) IFM-GEOMAR, Leibniz-Institut für Meereswissenschaften, Dienstgebäude Ostufer, Wischhofstr. 1-3, D-24148 Kiel, Germany
2) Centre de Sédimentologie-Paléontologie, FRE CNRS 2761 "Géologie des Systèmes Carbonatés", Université de Provence (Aix-Marseille I), 3, place Victor Hugo, Case 67, F-13331 Marseille Cédex 3, France
3) Present address: Vrije Universiteit, Faculty of Earth and Life Sciences (FALW), De Boelelaan 1085, 1081 HV Amsterdam, The Netherlands

[(*)] corresponding author: E-mail: John.Reijmer@falw.vu.nl

4) Marine Geology and Geophysics, Rosenstiel School of Marine and Atmospheric Science, 4600 Rickenbacker Causeway, Miami, Fl 33149
5) Present address:
   Schlumberger Oilfield Services D&M, Hamrasletta 15, 4056 Tananger, Norway
6) Present address:
   RWTH Aachen University, Wüllnerstr. 2, D-52062 Aachen, Germany
7) Present address:
   Nummerical Rocks, Stiklestadveien 1, 7041 Trondheim, Norway
8) Present address:
   TU Bergakademie Freiberg, Institut für Geologie und Paläontologie, Bernhardt-von-Cotta Straße 2, 09596 Freiberg, Germany

This is the accepted version of the following article: Reijmer, J.J.G., Swart, P.K.,Bauch, Th., Otto, R., Reuning, L., Roth, S. and Zechel, S. (2009): Facies maps of Great Bahama Bank. In: Perspectives in Sedimentary Geology: A Tribute to the Career of Robert Nathan Ginsburg (Eds. P.K. Swart, G.P. Eberli, J.A. McKenzie), IAS Spec. Publ. 41, p. 29-46, Wiley-Blackwell, ISBN:978-1-4051-9380-1

Running head: Facies Maps Western Great Bahama Bank

Abstract

A re-evaluation of the sediment distribution patterns on western Great Bahama Bank shows a facies distribution with two end-members. Coarse-grained sediments in the north, west, and south of the bank surround a mud-dominated realm located on the western leeward side of Andros Island. This facies distribution is comparable to earlier maps, but shows considerably more details and a complex distribution from grainstones to mud-rich wackestones. As in other carbonate platforms, sediment distribution appears to be influenced by (1) tidal currents, (2) prevailing wind direction, and (3) the interaction of the rate of Holocene sea-level rise with the pre-existing Pleistocene topography. The grain-size distribution very precisely reflects current–influenced and protected areas on the platform. The correlation between the distribution of pellets and the 63-125µm grain-size fraction most likely reflects the predominantly biological origin of this grain size. Aragonite dominates the mineralogy on the platform, low-magnesium calcite and high-magnesium calcite occurs in higher quantities only in a few environments on the platform.

Keywords: Facies distribution, Grain-size, Mineralogy, Great Bahama Bank, Holocene

INTRODUCTION

The Great Bahama Bank (Fig. 1A) has served as an inspiration for geologists in understanding modern processes of carbonate sedimentation since the pioneering work of Field (1931) and Illing (1954). Most of our knowledge of the spatial distribution of sediments on Great Bahama Bank (GBB) is based on the work of Illing (1954), Ginsburg et al. (1958), Newell et al. (1959), and Purdy (1963a,b). Valuable as these early descriptions are, it is the aim of this study to re-evaluate the distribution of the surface sediments on GBB using samples collected from precisely located points (Fig. 1B; established using GPS) and to quantify not only the types of sediments present, but also the mineralogy, grain-size distribution and skeletal and non-skeletal content. This paper together with a companion paper (Swart et al., this volume) takes a new look at the surface facies and geochemistry of sediments from Great Bahama Bank.

Various maps show sedimentary facies on GBB or in the Bahamas in general (Ginsburg et al., 1958; Newell et al., 1959; Purdy, 1963a,b; Ball, 1967; Enos, 1974). In all these studies sediments were classified using distinct facies types with comparable subdivisions. All maps show that skeletal sediments occur mainly on the margin of the bank whereas non-skeletal grains (mainly fecal pellets) dominate the interior of the platform. Very fine-grained sediments predominate in platform interior zones that are protected by topographic barriers such as marginal islands and submarine topography ("pelletoidal sands with lime mud matrix and lime muds", Ginsburg et al., 1958; "muddy sand and mud", Newell et al., 1959; "pellet-mud facies" and "mud facies", Purdy, 1963a; "pelletoidal packstones" and "pelletoidal wackestones", Enos, 1974). Some differences, however, exist in the interpretation and, as seen on the maps, in the distribution of the facies types. For example, Ginsburg et al. (1958) and Enos (1974) show that the sediments in the platform interior mainly contain pellets, peloids or pelletoids. Newell et al. (1959) and Purdy (1963a,b), however, described sediments containing a larger percentage of grapestones. Enos (1974) also described the occurrence of grapestones without showing them on the map as a particular facies type. Enos (1974) was the only study in which the Dunham classification (1962) was used and thus showed the components to matrix ratio along the platform. All maps known from the literature were based on sampling along a series of profiles crossing the bank and additional

datasets. All samples were taken without modern precision positioning systems and thus might contain significant uncertainties in the exact location of facies types.

The major question, however, concerns the processes that control the present facies distribution on western GBB, the Andros lobe. In this paper we try to determine the links between the sediment distribution and environmental parameters like currents, tides, topography, evaporation (salinity), precipitation, water exchange with the surrounding ocean water masses and sediment export.

Currents and circulation

Most of the surface water masses of the Caribbean Sea, which eventually form the Florida Current and the Gulf Stream, enter in the Lesser Antilles through various passages (Wajsowicz, 2002). A smaller portion (approximately 20%) enters the Caribbean Sea through the Windward Passage between Cuba and Hispaniola (Schmitz & Richardson, 1991). The Florida Current is fed as well by water masses through the Old Bahama Channel and Santaren Channel and through the Northwest Providence Channel (Fig. 1a; Leaman et al., 1995). Atkinson et al. (1995) and Leaman et al. (1995) showed that the average water transport through the Santaren Channel amounts to 1.9Sv or 1.8Sv, respectively. The transport through the Northwest Providence Channel reaches 1.2Sv (Leaman et al., 1995). On the western, leeward sides the current system on GBB is connected with the currents forming the sources of the Gulf Stream. On the windward sides a link exists with the North Atlantic Subtropical Gyre situated eastward in the Sargasso Sea. GBB has a great lateral extent and shows a well-defined marginal escarpment with islands. Shallow waters cover most of GBB and consequently, the interaction with water masses from the open ocean is limited (Smith, 1940). Islands like Andros Island deflect westward–moving currents generated by the trade winds to the north and south (Bathurst, 1975). As a result protected areas with limited water exchange are present on the western side of these islands (Bathurst, 1975). Water movement on GBB is mostly influenced by the wind and tides, but also by waves and storms (Smith, 1940; Cloud, 1962; Purdy, 1963a; Traverse & Ginsburg, 1966; Winland & Matthews, 1974; Gonzalez & Eberli, 1997).

Long-term net flow measurements over GBB showed a very slow current velocity of 2 cm/s toward the North (002 N; Smith,1995). This is thought to be the outcome of two almost opposing forces, a tide-induced flow toward the east-

southeast and a wind- and density-driven northward flow (Smith, 1995). Tidal currents vary from near 0 to 4 km/hr in the tidal channels (Newell & Rigby, 1957; Bathurst, 1975) and influence the entire platform to some degree.

Water temperature, wind and precipitation

The surface seawater temperature (SST) on GBB ranges from 18.5^{o}C during winter to 28.5^{o}C in summer (Cloud, 1962; Bathurst, 1975). During the summer higher SSTs are reached locally. Mixing of bank and ocean waters is very low (Purdy, 1963a). Smith (1940) noted that the difference in SST between bank and surface ocean waters may be as large as 3.6°C. The lateral variation in the SST on the bank itself is very low, but on bank margins the slow mixing with ocean water is demonstrated by changes in SST´s (Purdy, 1963a).

The Bahama Platform is influenced by the trade winds blowing from east or southeast in the summer (March to August). In the winter months, the winds have a north–easterly direction. Storms and hurricanes frequently visit the area, with winter storms generally coming from the northwest whereas the hurricane directions are highly variable. Only major storms affect sedimentation on the platform because of its great lateral extent and its protection by marginal shoals (rocky and sand shoals, and reefs) and islands (Tucker & Wright, 1990).

The annual precipitation over the Bahama Platform amounts to 1355 mm (Carew and Mylroie, 1997). The main part precipitates between May and November, with a maximum in September and October (Gebelein, 1974). The winter months (December-April) are relatively dry. The average monthly rainfall varies between 100 and 250mm (Miller et al., 1983).

Seasonal atmospheric circulation patterns strongly influence temperatures and precipitations of GBB. Circulation responds to changes in the position and strength of high and low pressure systems, the Intertropical Convergence Zone (ITCZ), the Subtropical Divergence Zone (STDZ), respectively, and the associated trade–wind belt. During May to November, the atmospheric highs and lows are less pronounced over the North Atlantic Ocean and the ITCZ and the STDZ move northward. The trade winds weaken and high precipitation prevails over the northern Bahamas. The atmospheric regime migrates southward during the boreal winter (December-April) and the ITCZ shifts toward the equator or slightly south of it (0–5°S). During this period the atmospheric high– and low–pressure systems strengthen and the easterly

trade winds are enhanced. The result is a stronger influence of colder and dryer air masses. During this winter period, the evaporation minus precipitation (E-P) averages around 225–250 cm/year while it only reaches about 50 cm/year in the summer (Smith, 1995).

Salinity

In summer, salinity varies from 36‰ near the edge of the platform to 46‰ in the platform interior, protected environment west of Andros Island (Smith, 1940; Ginsburg et al., 1958; Gebelein, 1974). Maximum winter salinity reaches 38‰ (Gebelein, 1974). Reasons for the persistence of increased salinity in the bank interior are the great lateral extension of the platform and the existence of marginal shoals and islands reducing the exchange of platform and open ocean waters (Tucker & Wright, 1990), Also during tides the exchange with oceanic water remains very small (Bathurst, 1975).

Carbonate mineralogy and grain size

Carbonate mineralogy at GBB is well documented and shows a dominance of aragonite on the platform top with minor high-magnesium calcite (HMC) and low-magnesium calcite (LMC) (Purdy, 1963a; Husseini & Matthews, 1972; Milliman, 1974; Mullins, 1986; Milliman et al., 1993).

Ginsburg (1956) noted, “Variations in the physical environment of carbonate depositional environments (bathymetry, areal geography, and hydrography) are reflected in the grain size and constituent particle composition of the sediments”. On the platform top grain size has been used as a relative indicator of current intensity (Purdy, 1963a). The *in situ* production of coarse-grained skeletal material and changes in the original particle size on the platform, e.g. grapestone formation and particle brackage, interfere with this assumption (Purdy, 1963a).

METHODS

Grab samples

Approximately 300 samples were obtained using a Shipek sampler during four cruises aboard the RV Bellows between 2001 and 2004 (Fig. 1B). The design of this

sampler prevents muds from escaping from the sample while being retrieved from the sea bottom It thus differs from the Van-Veen sampler used during earlier studies (Purdy, 1963a,b) in that it better retains the mud fraction.

Facies classification

Immediately after collection, samples were assigned to a modified Dunham scheme (Dunham, 1962). In order to complement the classification we added divisions between wackestone and mudstone (mud-rich wackestone; facies-no. 1.5), between a packstone and wackestone (mud-rich packstone, facies–no. 2.5), and finally between packstone and grainstone (mud-lean packstone or poorly-washed grainstone; facies-no. 3.5) (Fig. 2A). Samples from all cruises were preserved in cold storage and after the 2004 cruise all samples were re-examined to ensure consistency between cruises.

Grain-size variations

The samples were placed in 100ml containers and oven dried at 40°C before sieve analysis. A small split of the dried samples was analysed by X-ray diffraction. The dried samples were wet sieved to separate the coarse (>63μm) from the fine fraction (<63μm). The fine fraction was left in the 5 litre bottles to settle; water was then siphoned off; and the fine sediment was oven dried at 40ºC. The coarse fraction was dried, weighed and split into five sub–fractions (very coarse sand to gravel >1000µm; coarse sand, 500 – 1000µm; medium sand, 250 – 500µm; fine sand, 125 – 250µm; very fine sand, 63 – 125µm; after Wentworth, 1922) using a hand-held stainless–steel sieve set. Each sub-fraction was placed in a pre-weighed glass vial, which was weighed again, to determine the sub–fraction weight.

Mineralogy

Whole rock samples were oven dried at 40ºC and hand ground in a mortar to homogenize the sediment (Milliman, 1974). Additional samples representative of coarse and fine size fractions were similarly individually homogenized by grinding by hand in a mortar. The areas of the principal peaks of aragonite, HMC and LMC were measured with Scintag and Panalytical X-ray instruments using Cu-Kα radiation at RSMAS/University of Miami. The samples were scanned between 20º and 40º 2θ with a speed of 0.01º per second. The proportions of aragonite, HMC and LMC were

quantified using a method outlined by Swart et al. (2002) assuming that the sample is composed entirely of aragonite, HMC, and LMC, which is generally the case for GBB samples. The reproducibility of the method was determined through the replicate analysis of samples and is approximately +/- 2%.

Sediment composition

In order to identify individual facies groups, the coarse fraction (63 to >1000µm) of each sample was analyzed for its variation in skeletal (coral fragments, calcareous green algae, benthic foraminifera, gastropods, echinoderm spines and fragments, serpulids, ostracods, bryozoans, sponge spines and others) and non-skeletal components (peloids, ooids, grapestones, clasts) using a stereo binocular (sieve samples) as well as a polarizing microscope (thin-sections). Only the distribution of pellets and ooids is shown in this manuscript.

For the identification of the skeletal and non-skeletal components, the following literature was used: Bolli et al. (1994), Haq & Boersma (1978), Illing (1954), Flügel (2004), Loeblich & Tappan (1978), and Scholle & Ulmer-Scholle (2003).

RESULTS

Facies

The facies distribution (Fig. 2) shows a dominance of mud-free to mud-lean sediments in the north, west and south of the northern part of GBB. A gradual transition exists between these sediments and mud-rich wackestones present near the west side of Andros Island. The facies pattern is more complex compared to that presented in earlier studies (Ginsburg et al., 1958; Newell et al., 1959; Purdy, 1963b; Ball, 1967; Enos, 1974). A somewhat concentric distribution of various facies types is striking. The muddier sediment types (mud-rich wackestone (facies-no. 1.5) to packstone (facies-no. 3)) clearly dominate the platform interior. These sediments form a lobe adjacent to Andros Island, but also form an elongate zone close to the western edge of the platform. The cleaner sediments (packstones to grainstones) form a concentric belt on the western edge of the platform extending to the northern and southern regions. Remarkable features are the grainier tongues (facies-no. 3 and 3.5) projecting from NW-Andros Island in a WSW and WNW direction.

Grain-size

The grain-size distribution on GBB shows a distinct trend from coarse sediments on the western edge of the platform towards finer and muddier sediments in the vicinity of Andros Island (Fig. 3A-D). The tidal flats with scrub mangroves on the western side of Andros Island further confirm the muddy character of the sediments in this inner platform environment. The coarsest mean grain-sizes are on the northern, western, and southern margins of the bank. The mean grain-size map (Fig. 3A) precisely displays open and protected environments on the platform. Note especially the zones with relatively coarse-grained sediments associated with the ooid belts at the eastern edge of the platform, N and SSE of Andros Island, near the Tongue of the Ocean.

Mineralogy

Aragonite is by far the dominant mineral across the platform and varies between 77.7 and 100%, with a mean of 93.3% (Fig. 4A; Table 1). High- and low-magnesium calcite (HMC and LMC) content varies between 0 and 22.3%, and 0 and 3.9%, respectively, with a mean of 6.5% for HMC and 0.2% for LMC (Fig. 4B, 4C; Table 1). The analysis of the fine-fraction (<63 µm) of the 2004 dataset showed an appreciable increase in the mean values of HMC and LMC, with values ranging from 4.8% (bulk samples) to 10.6 % (fine fraction) for HMC and from 0.5 % (bulk) to 6.7 % (fine fraction) for LMC (Table 1).

Facies variations

The distribution of pellets largely coincides with the mud-rich facies distribution; they are more abundant in restricted areas of the platform (Fig. 5A). As might be expected, ooids preferentially occur on the edge of the platform and in the more open areas on the platform (south and north of Andros Island; Fig. 5B) and thus show a large overlap with the more grainy facies types on the platform. The largest quantities of *Halimeda sp.* were present in deeper waters, on the northern edge of the platform. On the platform itself *Halimeda sp.* only occurs in minor quantities. Grapestones were found on the more open northern part of the platform and along the southern side of the investigated area (not shown). Part of the grapestones from the northern sector of the platform consist of non-indurated grains bound by soft algal

mucus that thus differ from the indurated ones found in the southern part of the platform.

DISCUSSION

Two major questions should be answered when discussing the sediment distribution along GBB: (i) what physical and biological processes control the present-day sediment distribution? (ii) How does this distribution compare with facies distribution patterns observed on other carbonate platforms? We will discuss possible links between sediment distribution and physical processes like currents, tides, platform topography, evaporation (salinity), water exchange with the surrounding ocean water masses, and sediment export.

Facies patterns

Purdy (1963b) hypothesized that the facies on GBB theoretically would be distributed in a series of bilaterally symmetrical bands parallel to the margin of the bank. However, the depositional topography of the Pleistocene substrate created local current conditions that have resulted in the somewhat patchy facies distribution pattern observed (Purdy, 1963a,b). The early maps of Newell & Rigby (1957) and Newell et al. (1959), however, showed some concentric facies belts in the lee of Andros Island.

All samples taken during these early studies were taken by hand or using a Van Veen grab-sampler. The Van-Veen sampler has the disadvantage that it looses a proportion of the very fine fraction (<63µm) during the retrieval process. This probably is the reason that differences in the mud content exist between the early facies maps and our data. The distribution pattern observed in our study of GBB, however, shows a roughly concentric series of facies belts with an outer edge dominated by coarse-grained, mud-free to poorly washed grainstones, and an inner platform area with mud-rich wackestones forming an U-shaped band, situated close to Andros Island (Fig. 2).

Rankey & Morgan (2002) and Rankey (2002) suggested that the tidal flats west of Andros Island do not respond solely to the rate of sea-level rise, but also to the variation in circulation or storm intensity and direction. The tongue of less muddier sediment that extends from northwest Andros Island supports this scenario because it is clearly positioned at a location where the influx of waters from the east

was observed on this side of the platform (Newell & Rigby, 1957; Harris, 1979, 1983). Another factor that seems to influence the distribution of mud-rich sediments is water depth and the related parameter, water energy. Mud-rich aragonitic sediments characterize the deeper areas while the shallower areas comprise coarser-grained sediments. As shown on the facies map (Fig. 2), Andros Island plays also an important role in the present-day sediment distribution as it protects the inner–platform environments from the currents induced by the easterly trade winds and by tides. The facies change to predominantly grainstones (Facies-no. 3.5 to 4) observed north and south of Andros Island precisely registers the influence of currents on the overall sediment distribution. The ooid-dominated tidal bars south of Tongue of the Ocean (Ginsburg, 2005) and north of Andros Island, on Joulters Cay (Newell & Rigby, 1957; Ball, 1967; Harris, 1979, 1983), also support the presence of strong currents that enter the shallow-water environments. The mud-free facies is positioned close to these facies belts, and thus confirms the influence of currents on the grain-size distribution in these parts of the platform. The grainstone belt (Facies no. 4) crossing the platform south of Andros Island suggests that this zone acts as a conduit for currents of Tongue of the Ocean water. Another interesting feature is the agreement between the pellet distribution and the abundance of the 63-125µm grain-size fraction showing the biological control on grain-size distribution (Compare Fig. 3C and 5A).

Another process that influences the facies distribution are the tidal currents that freely enter the shallow-water platform. This is shown by the trend towards mud-free sediments in the southern part of the platform where no major barriers exist that would prevent the removal of the fine-grained material (Fig. 2, 3A, 3B, 3D). The observed export of shallow-water muds by physical processes occurring during passage of winter cold fronts confirms this inference (Wilson & Roberts, 1992, 1995). The precise correlation of variations in sediment accumulation on the western slope of GBB with the scaling of atmospheric and oceanographic processes underlines the subtle character of the processes influencing sediment export from the inner platform areas (Roth & Reijmer, 2004, 2005).

Topography and sediment distribution

Another important question is whether the platform topography inherited from the last glacial cycle influenced the facies distribution pattern found today. The

present-day distribution shows a link between water depth on the platform and the type of sediment present. Mud-rich facies (facies-no. 1.5) shows a clear relation to deeper areas (Fig 2). Coarse-grained, mud-free facies occur either close to the edge of the platform, or on elevated areas within the interior of the platform (e.g. southeast of Bimini; Fig. 1, 3A-D), or within the more open parts of the platform, in the southern part of the study area. Newell et al. (1959) described two broad shoals running across the Andros lobe, (i) the Bimini axis, which extends from Bimini in the west to the northern tip of Andros Island, and (ii) the Billy Island axis running westward from the middle promontory of Andros Island. The map of mean grain-size reflects these topographic features (Fig. 3A). The more open character of the southern part of the platform is also clearly shown by coarser, cleaner sediments on these maps (Fig. 3A-D). Tidal currents entering the platform in combination with wave action most likely caused this distribution.

Comparisons with other platform lagoons

Other carbonate platform lagoons like those from Mayotte in the Indian Ocean (Zinke et al. 2001, 2003a), show a facies distribution pattern that is clearly influenced by the interplay of the antecedent topography and the rate of the Holocene sea-level rise (Zinke et al., 2003b, 2005). The rate with which the former topography was flooded determined the development of a current pattern within the lagoon and thus steered facies distribution. This current pattern also depended on the continuity of the barrier surrounding the lagoon before the platform interior was reflooded after the last glacial. Other present-day facies variations were related to either the vicinity of the barrier reef or the reefs surrounding the inner lagoon of the island or the input of terrigenous material. The link between facies variations and the distance to the edge of the platform also can be observed on the Bahamian platform. The same holds for the influence of the antecedent topography (see discussion below).

In a discussion of the sediment distribution of three isolated carbonate platforms seaward of the Belize barrier reef system (Glovers Reef, Lighthouse Reef and Turneffe Islands) Gischler (1994) and Gischler & Lomando (1999) suggested that variations in antecedent topography and exposure to waves and currents were the dominant factors influencing the sediment distribution of these three relatively small-scale carbonate platforms. In analogy with the scenario developed for the facies distribution of the inner lagoon of Mayotte (Zinke et al., 2001, 2003a), Gischler

(2003) showed that the timing of reflooding of the Pleistocene bedrock in combination with the rate of sea-level rise determined the sedimentation patterns in the lagoons of the Belize atolls. The early flooded atolls (Glovers Reef and Lighthouse Reef) developed an open-circulation pattern, while the Turneffe Islands, flooded in a relatively late stage, at present has restricted circulation. The latter might also be related to its present rather low-energy position in the lee of the other platforms. Purdy & Gischler (2003) also noted that the distribution and overall character of the Holocene facies in the lagoons of Belize is strongly influenced by processes like siliciclastic input related to the uplift of the hinterland, and by antecedent topography of structural origin influenced by karst processes during glacial lowstands (Purdy, 1974; Purdy et al., 2003).

The data available on the antecedent pre-Holocene topography of GBB (Boss & Rasmussen, 1985; Boss, 1996), also suggest that the observed facies patterns to some extent link to the antecedent topography. The correlation between the timing of the last sea-level rise flooding the shallow-water areas of the platform and the onset of sediment production, without any significant lag time, suggests that the antecedent pre-Holocene topography acted as sediment production and export site immediately after reflooding (Roth & Reijmer, 2004).

The facies distribution shows the interaction of the prevailing winds and currents with the pre-existing topography. At present considerable accommodation space is unfilled, which probably results from a combination of a pre-existing topography, flat-topped platform with no distinct barrier, and a rate of sea-level rise that resulted in the establishment of a current system removing sediment, soon after the platform was flooded. This early export of platform sediments towards the surrounding slopes and basins started at 7.2ka BP, shortly after reflooding of the shallow-water areas, as discussed by Wilber et al. (1990), McNeill et al. (1998), and Roth & Reijmer (2004, 2005).

Mineralogy

Appreciable differences exist between the carbonate mineralogy of the bulk sediments (Fig. 4) and the <63µm grain-size fraction (not shown). The percentage of HMC and LMC increases in the <63µm fraction when compared with the bulk sediments (Table 1). These differences are most likely related to the export of the fine aragonite muds produced in the water column, the so-called whitings (Shinn et

al., 1989; Robbins & Blackwelder, 1992; MacIntyre & Read, 1992, 1995; Milliman et al., 1993; Thompson et al., 1997; Yates & Robbins, 1998, 1999). This production of aragonite fines in the water column makes them very sensitive to transport during tides, storms and passing winter fronts (McCave, 1972; Neumann & Land, 1975; Wilson & Roberts, 1992, 1995; Wilber et al., 1993). The precise recording of climatic variations on the slopes of GBB most likely reflects this process (Roth & Reijmer, 2005).

HMC shows highest values along the northern edge of the platform (Fig. 4B). Slightly increased values occur in the mud-dominated facies belt in the lee of Andros Island. The cause of this latter increase remains uncertain, but could have a biologic (e.g. pellet formation) or a diagenetic origin

Two small zones with slightly elevated LMC values occur on the bank (Fig. 4C). One near the western tip of Andros, which is probably related to the input of Pleistocene eroded material from the island. The second zone relates to an inlet on the eastern side of the platform in which the ooid shoals occur also, evidencing strong currents that enter the platform from the Tongue of the Ocean.

Facies patterns and isotope signals

Mud-dominated, aragonite-rich sediments (facies types 1.5 to 4.5) form the majority of the sediments in the interior of GBB (Fig. 2, 3A, 4A). These facies belts are surrounded by skeletal and non-skeletal aragonite sediments on the northern and western outer edges of the platform and in the southern parts of the study area (Fig. 2). The predominantly aragonite sediments on GBB have similar $\delta^{13}C$ and $\delta^{18}O$ compositions (Swart et al., this volume). A comparison between the pellet distribution and the distribution of the mud-rich sediments (compare Fig. 2, 3C and 5A) shows that muds and related sediment particles are important sediment components on the platform. The muds and their derivates seem to dominate the isotope distribution observed on GBB (Swart et al., this volume).

Comparison between new facies map and literature data

The facies maps that are widely used in the literature are based on the data sets presented by Illing (1954), Ginsburg et al. (1958; Fig. 6A), Newell & Rigby (1957), Newell et al. (1959), Cloud (1962), Purdy (1963a), and Traverse & Ginsburg (1966; Fig. 6A). The most widely used facies distribution maps of Purdy (1963b; Fig.

6B) and Enos (1974; Fig. 6C) make use of these data sets. The facies, grain-size and mineralogy maps presented in this study show a more diverse distribution of all sediment parameters along the platform. The gross facies distribution with a skeletal-dominated, coarse-grained platform edge and a mud-dominated interior in the lee of Andros Island shows up on all maps, however (Fig. 2, 6A-C). Another feature that shows up on all maps is the sharp transition from mud-dominated sediments (facies-type 1.5) to grainstone facies (facies type 4) on the western boundary of the platform (Fig. 2, 6A-C). A detailed comparison, however, is difficult, because the majority of the maps use a classification scheme partly based on the occurrence of single grain types and carbonate muds. A significant difference is that the dominant grapestone occurrence in the northern part of the platform as shown by Newell et al. (1959) and Purdy (1963b) could not be confirmed by our study (compare Fig. 2 with 6B). On the Enos (1974) map this northern grapestone-dominated facies belt was classified as a peloid dominated grainstone facies, which agrees more with our results (compare Fig. 2 with Fig. 6C). Despite the fact that the Enos (1974) map also uses the Dunham classification scheme (1962), large differences in facies distribution exist between that map and this study. Further detailed studies on the composition of the different grain-size fractions in combination with a detailed petrographic analysis are needed to quantify the skeletal and non-skeletal component distribution on the platform.

CONCLUSIONS

The facies, grain-size and mineralogy distribution patterns on GBB show a current-dominated sedimentation pattern with a clear distinction between the outer edge and the inner platform. Inner-platform facies distribution relates to the present-day bathymetry, which might represent in part an inherited Pleistocene topography. Seismic studies are needed to verify this.

Grain-size differences reflect the bottom topography and show a more coarse-grained outer platform and a mud-dominated interior. The grainstone distribution north and south of Andros Island registers the presence of strong currents that enter and cross the shallow-water environment. The correlation between the distribution of the 63-125µm grain-size fraction and the distribution of pellets suggests a predominantly biological origin of this grain size.

The mineralogy of the sediments shows a clear dominance of aragonite mixed with HMC and minor LMC. Concentration of calcite (HMC, LMC) in the fine fraction

suggests a preferential transport of aragonite-rich muds from the platform through various processes.

ACKNOWLEDGEMENTS

The authors thank the crew of the RV *Bellows* for their assistance gathering this data set throughout four cruises between 2001 and 2004. We also thank Jill Falk, Hendrik Lantzsch and Astrid Ryba (Kiel) and Amel Saied and Corey Schroeder (Miami) for their help preparing the samples. This project was funded in part by the German Science Foundation (Projects Re1051/8 and 9) and Leibniz funds of W.-Chr. Dullo (IFM-GEOMAR, Kiel). Additional support for the use of the RV *Bellows* was provided by Florida Institute of Oceanography and Comparative Sedimentology Laboratory. We thank Paul (Mitch) Harris, Pascal Kindler and Paul Enos for their constructive reviews of the manuscript.

REFERENCES

Atkinson, L.P., Berger, T., Hamilton, P., Waddell, E., Leaman, K. and **Lee, T.N.** (1995) Current meter observations in the Old Bahama Channel. *J. Geophys. Res.*, **100**, 8555-8560.

Ball, M.M. (1967) Carbonate sand bodies of Florida and the Bahamas**.** *J. Sed. Petrol*., **37(2)**, 556–591.

Bathurst, R.G.C. (1975) *Carbonate sediments and their diagenesis*. Developments in sedimentology, **12**. Elsevier, Amsterdam, 439 pp.

Bolli, H.M., Beckmann, J.-P. and **Saunders, J.B.** (1994) Benthic foraminiferal biostratigraphy of the South Caribbean Region. Cambridge Univ. Press, 408 pages.

Boss, S.K. (1996) Digital shaded relief image of a carbonate platform (northern Great Bahama Bank): scenery seen and unseen. *Geology*, **24**, 985-988.

Boss, S.K. and **Rasmussen, K.A.** (1995) Misuse of Fischer plots as sea-level curves. *Geology*, **23**, 221-224.

Carew, J.L. and **Mylroie, J.E.** (1997) Geology of the Bahamas. In: Geology and Hydrogeology of Carbonate Islands (Eds H. L. Vacher and T. M. Quinn), pp. 91–139. Elsevier Science, New York, U.S.A.

Cloud Jr, P.E. (1962) Environment of calcium carbonate deposition west of Andros Island. *U.S. Geol. Surv. Profess. Papers*, **350**, 1-138.

Dunham, R.J. (1962) Classification of carbonate rocks according to depositional texture. In: Classification of carbonate rocks – A symposium (Ed. W.E. Ham), *AAPG Memoir* **1**, pp. 108-121. American Association of Petroleum Geologists, Tulsa, Oklahoma, U.S.A.

Enos, P. (1974) Surface sediment facies of the Florida-Bahamas Plateau Map Series MC-5 no.4 edn. Geological Society of America, Boulder, Colorado, U.S.A.

Field, R.M. (1931) Geology of the Bahamas. *GSA Bull.*, **42**: 759-784.

Flügel, E. (2004) *Microfacies of carbonate rocks*. Springer, Berlin, Germany, 976 pp.

Gebelein, C.D. (1974) Guidebook for modern Bahamian platform environments. Geol. Soc. Am. Ann. Mtg Field Guide, 93 pp. Geological Society of America, Boulder, Colorado, U.S.A.

Ginsburg, R.N. (1956) Environmental relationships of grain size and constituent particles in some South Florida carbonate sediments. *AAPG Bull.*, **40**: 2384-2427.

Ginsburg, R.N., Lloyd, R.M., McCallum, J.S., Stockman, K.W. and **Moody, R.A.** (1958) Surface sediments of Great Bahama Bank, Shell Development Company, Houston, Texas, USA.

Ginsburg, R.N. (2005) Disobedient sediments can feedback on their transportation, deposition and geomorphology. *Sed. Geol.*, **175**: 9 –18.

Gischler, E. (1994) Sedimentation on three Caribbean atolls: Glover Reef, Lighthouse Reef and Turneffe Islands, Belize. *Facies*, **31**: 243-254.

Gischler, E. (2003) Holocene lagoonal development in the isolated carbonate platforms off Belize. *Sed. Geol.*, **159**: 113-132.

Gischler, E. and **Lomando, A.J.** (1999) Recent sedimentary facies of isolated carbonate platforms, Belize-Yucatan system, Central America. *J. Sed. Res.*, **69**: 747-763.

Gonzalez, R. and **Eberli, G.P.** (1997) Sediment transport and bedforms in a carbonate tidal inlet; Lee Stocking Island, Exumas, Bahamas. *Sedimentology*, **44**: 1015-1030.

Haq, B.U. and **Boersma, A.** (1978) *Introduction to marine micropaleontology*. Elsevier - New York, 376 pp.

Harris, P.M. (1979) Facies anatomy and diagenesis of a Bahamian ooid shoal. *Sedimenta*, **7**: 175.

Harris, P.M. (1983) The Joulters ooid shoal, Great Bahama Bank. In: *Coated grains* (Ed. T.M. Peryt), pp. 132-141. Springer, Berlin, Heidelberg, Germany.

Husseini, S.I. and **Matthews, R.K.** (1972) Distribution of high-magnesium calcite in lime muds of the Great Bahama Bank; diagenetic implications. *J. Sed. Petrol.*, **42(1)**, 179-182.

Illing, L.V. (1954) Bahaman calcareous sands. *AAPB Bull.*, **38**: 1-95.

Leaman, K.D., Vertes, P.S., Atkinson, L.P., Lee, T.N., Hamilton, P. and **Waddell, E.** (1995) Transport, potential vorticity, and current/temperature structure across Northwest Providence and Santaren Channels and the Florida Current off Cay Sal Bank. *J. Geophys. Res.*, **100**: 8561-8569.

Loeblich, A.R. Jr. and **Tappan, H.** (1978) Sarcodina chiefly "Thecamoebians" and Foraminiferida. In: Treatise on invertebrate paleontology, part C, Protista 2 (Ed. R.C. Moore). Geological Society of America and University of Kansas Press, Vol. 1/2. Geological Society of America, Boulder, Colorado, U.S.A.

MacIntyre, I.G. and **Reid. R.P.** (1992) Comment on the origin of aragonite needle mud: A picture is worth a thousand words. *J. Sed. Petrol*., **62(6)**, 1095–1097.

MacIntyre, I. G. and **Reid, R. P.** (1995) Crystal alteration in a living calcareous alga (Halimeda): Implications for studies in skeletal diagenesis, *J. Sed. Res.*, **A65**, 1143–1153.

McCave, I.N. (1972) Transport and escape of fine-grained sediment from shelf areas. In: Shelf Sediment Transport (Eds D. J. P. Swift, D. B. Duane and O. H. Pilkey), pp. 225–248. Van Nostrand Reinhold, New York, U.S.A.

McNeill, D., Grammer, G.M. and Williams, S.C. (1998) A 5 My chronology of carbonate platform margin aggradation, southwestern Little Bahama Bank, Bahamas. *J. Sed. Res.*, **68**, 603-614.

Miller, A., **Thompson, J.C.**, **Peterson**, **R.E.** and **Haragan, D.R**. (1983) Elements of meteorology. 4th ed. Columbus (Merill Publ. Co.), U.S.A.

Milliman, J.D. (1974) *Marine carbonates*. Springer Verlag, Berlin-Heidelberg-New York, 375 pp.

Milliman, J.D., Freile, D., Steinen, R. and Wilber, R.J. (1993) Great Bahama Bank aragonitic muds: mostly inorganically precipitated, mostly exported. *J. Sed. Petrol*, **63(4)**, 589-595.

Mullins, H.T. (Ed) (1986) *Carbonate depositional environments, modern and ancient. Part 4: periplatform carbonates*. (Eds J.E. Warme and K.W. Shanley), *Quarterly*, **81**, pp 1-63. Colorado School of Mines Press, Golden (Colorado), U.S.A.

Neumann, A.C. and **Land, L.S.** (1975) Lime mud deposition and calcareous algae in

the Bight of Abaco, Bahamas: a budget. *J. Sed. Petr.*, **45**: 763-786.

Newell, N.D. and Rigby, J.K. (1957) Geological studies on the Great Bahama Bank. In: *Regional aspects of carbonate deposition: A symposium with discussion* (Eds R.J. Le Blanc and J.G. Breeding), SEPM Spec. Publ., **5**, pp. 15-72. Society of Economic Paleontologists and Mineralogists, Tulsa, Oklahoma, U.S.A.

Newell, N.D., Imbrie, J., Purdy, E.G. and **Thurber, D.L.** (1959) Organism communities and bottom facies, Great Bahama Bank. *Bull. Am. Museum. Nat Hist.*, **117**: 177-228.

Purdy, E.G. (1963a) Recent calcium carbonate facies of the Great Bahama Bank. 1. Petrography and reaction groups. *J. Geol.*, **71**: 334-355.

Purdy, E.G. (1963b) Recent calcium carbonate facies of the Great Bahama Bank. 2. Sedimentary facies. *J. Geol.*, **71**: 472-497.

Purdy, E.G. (1974) Karst-determined facies patterns in British Honduras: Holocene carbonate sedimentation model. *AAPG Bull.*, **58**, 825-855.

Purdy, E.G. and Gischler, E. (2003) The Belize margin revisited: 1. Holocene marine facies. *Int. J. Earth Sci. (Geol. Rundsch.)*, **92**: 532–551.

Purdy, E.G., Gischler, E. and **Lomando, A.J.** (2003) The Belize margin revisited. 2. Origin of Holocene antecedent topography. *Int. J. Earth Sci. (Geol. Rundsch.)*, **92**: 552–572.

Rankey, E.C. (2002) Spatial patterns of sediment accumulation on a Holocene carbonate tidal flat, Northwest Andros Island, Bahamas. *J. Sed. Res.*, **72**: 591-601.

Rankey, E.C. and **Morgan, J.** (2002) Quantified rates of geomorphic change on a modern carbonate tidal flat, Bahamas. *Geology*, **30**: 583-586.

Robbins, L.L. and **Blackwelder, P.L.** (1992) Biochemical and ultrastructural evidence for the origin of whitings: A biologically induced calcium carbonate precipitation mechanism. *Geology*, **20**: 464– 468.

Roth, S. and **Reijmer, J.J.G.** (2004) Holocene Atlantic climate variations deduced from carbonate periplatform sediments (leeward margin, Great Bahama Bank). *Paleoceanography*, **19**: PA1003, doi:10.1029/2003PA000885.

Roth, S. and **Reijmer, J.J.G.** (2005) Holocene millennial to centennial carbonate cyclicity recorded in slope sediments of the Great Bahama Bank and its climatic implications. *Sedimentology*, **52**: 161–181.

Schmitz, W.J. and **Richardson, P.L.** (1991) On the sources of the Florida Current. *Deep-Sea Res.*, **38**, 379-401.

Scholle, P.A. and Ulmer-Scholle, D.S. (2003) *A color guide to the petrography of carbonate rocks*, AAPG Memoir**, 77**. American Association of Petroleum Geologists, Tulsa, Oklahoma, U.S.A.

Shinn, E.A., Steinen, R.P., Lidz, B.H. and **Swart, P.K.** (1989) Whitings, a sedimentologic dilemma. *J. Sed. Petrol.*, **59**: 147-161.

Smith, C.L. (1940) The Great Bahama Bank. *J. Mar. Res.*, **3**, 147-189.

Smith, N.P. (1995) On long-term net flow over Great Bahama Bank. *J. Phys. Oceanogr.*, **25**, 679– 684.

Swart, P.K. James, N.P., Mallinson, D., Malone, M.J., Matsuda, H. and **Simo, T**. (2002) Data report: Carbonate mineralogy of sites drilled during Leg 182, In: *Proceedings of the Ocean Drilling Program, Scientific Results* (Eds. A.C. Hine, D.A. Feary and M.J. Malone), **182** (CD Rom). ODP, College Station, Texas, U.S.A.

Swart, P.K., **Reijmer, J.J.G.** and **R. Otto** (this volume) A reevaluation of Facies on Great Bahama Bank II: Variations in the $\delta^{13}C$, $\delta^{18}O$, and mineralogy of surface sediments on Great Bahama Bank In: *Perspectives in Sedimentary Geology: A Tribute to the Career of Robert Nathan Ginsburg* (Eds. P.K. Swart, G.P. Eberli and J.A. McKenzie), IAS Special Publication. Blackwell, Oxford.

Thompson, J.B., Schultze-Lam, S., Beveridge, T. J. and **Des Marais, D.J.** (1997) Whiting events: Biogenic origin due to the photosynthetic activity of cyanobacterial picoplankton. *Am. Soc. Limnol. Oceanogr.*, **42(1)**, 133–141.

Traverse, A. and **Ginsburg, R.N.** (1966) Palynology of the surface sediments of Great Bahama Bank, as related to water movement and sedimentation. *Mar. Geol.*, **4**: 417-459.

Tucker, M.E. and **Wright, V.P.** (1990) *Carbonate sedimentology*. Blackwell Scientific Publications, Oxford, UK, 482 pp.

Wajsowicz, R.C. (2002) A modified Sverdrup Model of the Atlantic and Caribbean circulation. *J. Phys. Oceanogr.*, **32**, 973-993.

Wenthworth, C.K. (1922) A scale of grade and class terms for clastic sediments. J. Geol., **30**, 377-392.

Wilber, R.J., Milliman, J.D. and **Halley, R.B.** (1990) Accumulation of bank-top sediment on the western slope of Great Bahama Bank: rapid progradation of a carbonate megabank. *Geology*, **18**: 970-974.

Wilber, R.J., Whitehead, J., Halley, R.B. and **Milliman, J.D.** (1993) Carbonate periplatform sedimentation by density flows: A mechanism for rapid off-bank and

vertical transport of shallow-water fines: Comment and reply. *Geology*, **21**: 667–669.

Wilson, P.A. and **Roberts, H.H.** (1992) Carbonate-periplatform sedimentation by density flows: a mechanism for rapid off-bank and vertical transport of shallow-water fines. *Geology*, **20**: 713-716.

Wilson, P.A. and **Roberts, H.H.** (1995) Density cascading: off-shelf sediment transport, evidence and implications, Bahama Banks. *J. Sed. Res.*, **A65**: 45-56.

Winland, H.D. and **Matthews, R.K.** (1974) Origin and significance of grapestone, Bahama Islands. *J. Sed. Petrol.*, **44**, 3, 921-927.

Yates K. K. and **Robbins L. L.** (1998) Production of carbonate sediments by a unicellular green alga. *Amer. Mineralogist* **83,** 1503– 1509.

Yates, K.K. and **Robbins, L.L.** (1999) Radioisotopic tracer studies of inorganic carbon and Ca in microbially derived $CaCO_3$. *Geochim. Cosmochim. Acta*, **63**: 129-136.

Zinke, J., Reijmer, J.J.G. and **Thomassin, B.A.** (2001) Seismic architecture and sediment distribution within the Holocene barrier reef-lagoon complex of Mayotte (Comoro archipelago, SW Indian Ocean). *Palaeogeo., Palaeoclim., Palaeoecol.*, **175**: 343-368.

Zinke, J., Reijmer, J.J.G. and **Thomassin, B.A.** (2003a) Systems tracts sedimentology in the lagoon of Mayotte associated with the Holocene transgression. *Sed. Geol.*, **160**: 57-79.

Zinke , J., Reijmer, J.J.G., Thomassin, B.A., Dullo, W.-C., Grootes, P.M. and **Erlenkeuser, H.** (2003b) Postglacial flooding history of Mayotte Lagoon (Comoro Archipelago, southwest Indian Ocean). *Mar. Geol.*, **194**: 181-196.

Zinke, J., Reijmer, J.J.G., Taviani, M., Dullo, W.-C. and **Thomassin, B.A.** (2005) Facies and faunal assemblage changes in response to the Holocene transgression in the lagoon of Mayotte (Comoro Archipelago, SW Indian Ocean). *Facies*, **50**: 391–408.

Table

Table 1. Fractional abundance of carbonate mineralogies (% of total carbonate).

Figure captions

Figure 1.

A. Location map of Great Bahama Bank with main topographic names. Old BHM Channel: Old Bahama Channel.

B. Location map samples (yellow crosses). Satellite image of Great Bahama Bank shows the shallow-water bank in light blue to green colours. Deep-water basins show up in dark blue colours. Morphology of the islands accentuated in yellow. Large island in the centre of the figure is Andros Island. Latitude and longitude indicated at the side. Km-bar for scale.

Figure 2.

Facies distribution along Great Bahama Bank. Mud-rich wackestone = 1.5; Wackestone = 2; Mud-rich packstone = 2.5; Packstone = 3; Mud-lean packstone or poorly-washed grainstone = 3.5; Grainstone = 4; Rudstone = 5.

Figure 3.

Grain-size distribution across Great Bahama Bank. A. Mean Grain-size; B. Grain size < 63μm (% of total sample); C. 63-125μm (% of total sample); D. Grain size 500-1000 μm (% of total sample).

Figure 4.

Mineralogy distribution along Great Bahama Bank (bulk samples). A. Fractional abundance Aragonite (bulk samples); B. Fractional abundance HMC (bulk samples); C. Fractional abundance LMC (bulk samples). 1.0 represents 100%.

Figure 5.

Presence (shaded areas) on Great Bahama Bank of (A) pellets and (B) ooids.

Figure 6.

A. Facies map (modified) after Ginsburg et al. (1958) and Traverse & Ginsburg (1966); B. Facies map (modified) after Purdy (1963b); C. Facies map (modified) after Enos (1974).

Table 1. Fractional abundance of carbonate mineralogies (% of total carbonate)									
	Bulk Total Dataset			Bulk 2004 Dataset			<63 μm 2004 Dataset		
	Mean	Max.	Min.	Mean	Max.	Min.	Mean	Max.	Min.
Aragonite	93.3	100	77.7	94.8	100	79,9	82.7	94.5	36.5
HMC	6.5	22.3	0	4.8	19.5	0	10.6	20.3	2.8
LMC	0.2	3.9	0	0.5	1.6	0	6.7	47.2	0.4

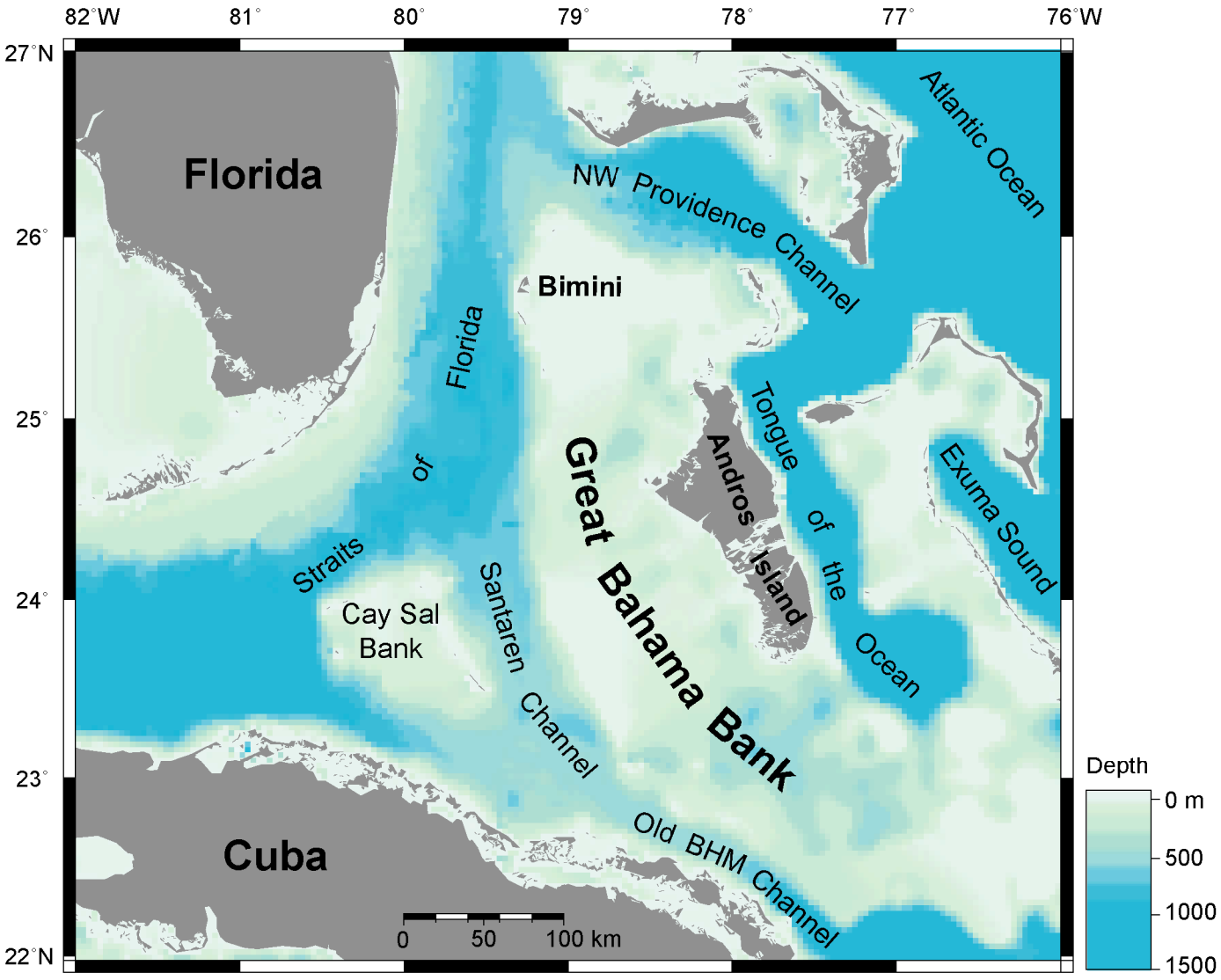

Reijmer et al.
Figure 1A. Location map

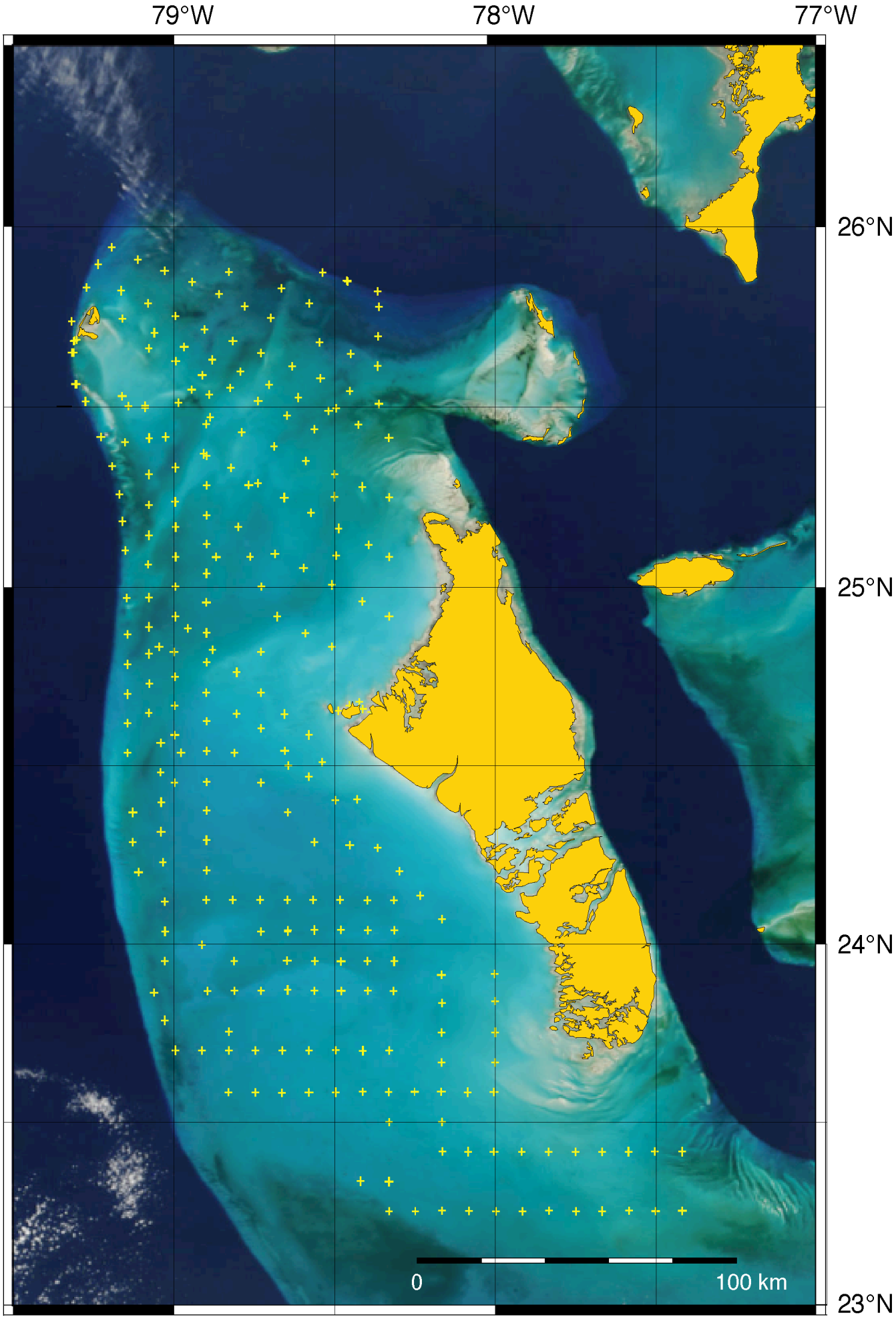

Reijmer et al.:
Figure 1B. Location map sampling points

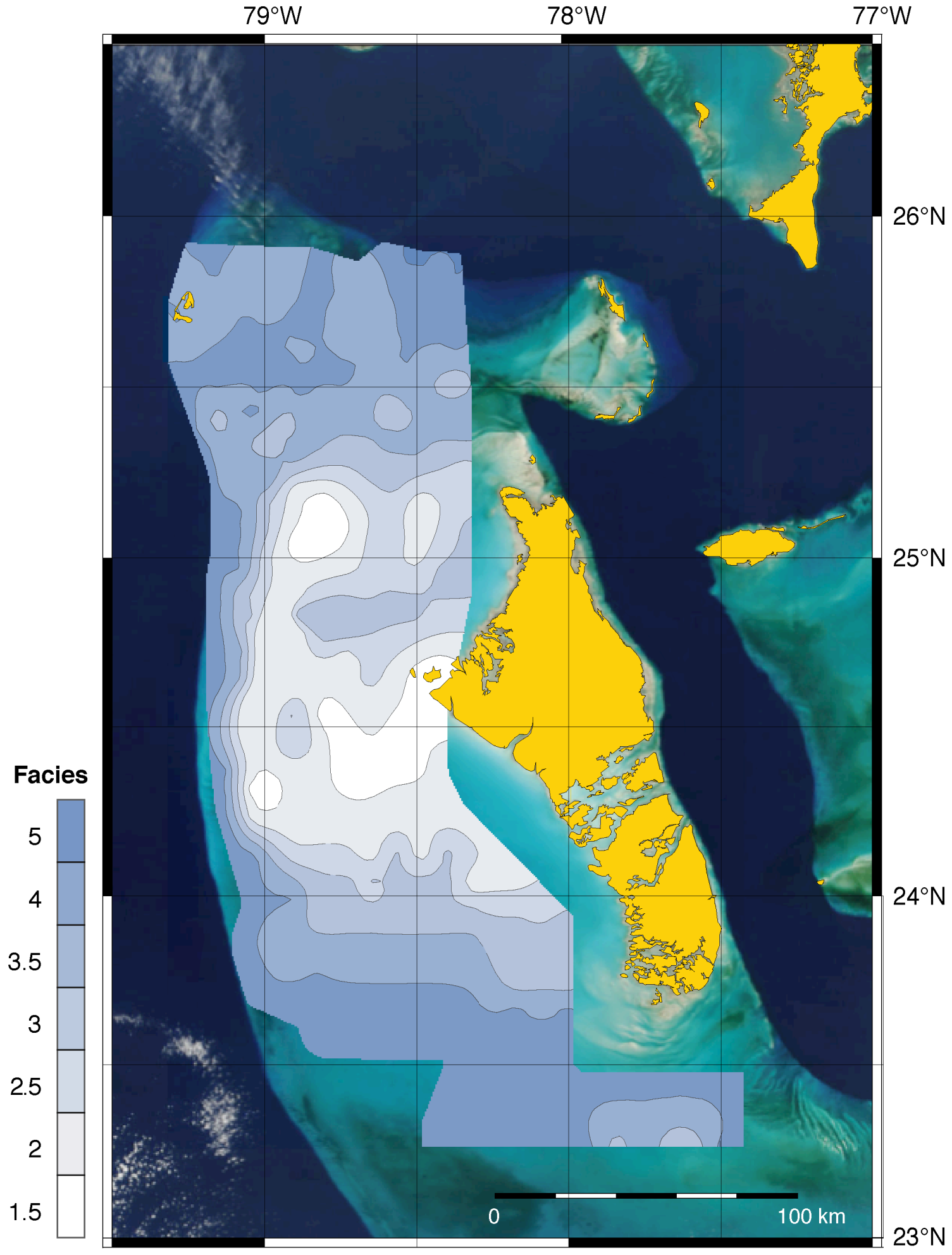

Reijmer et al.
Fig. 2 Facies distribution map.

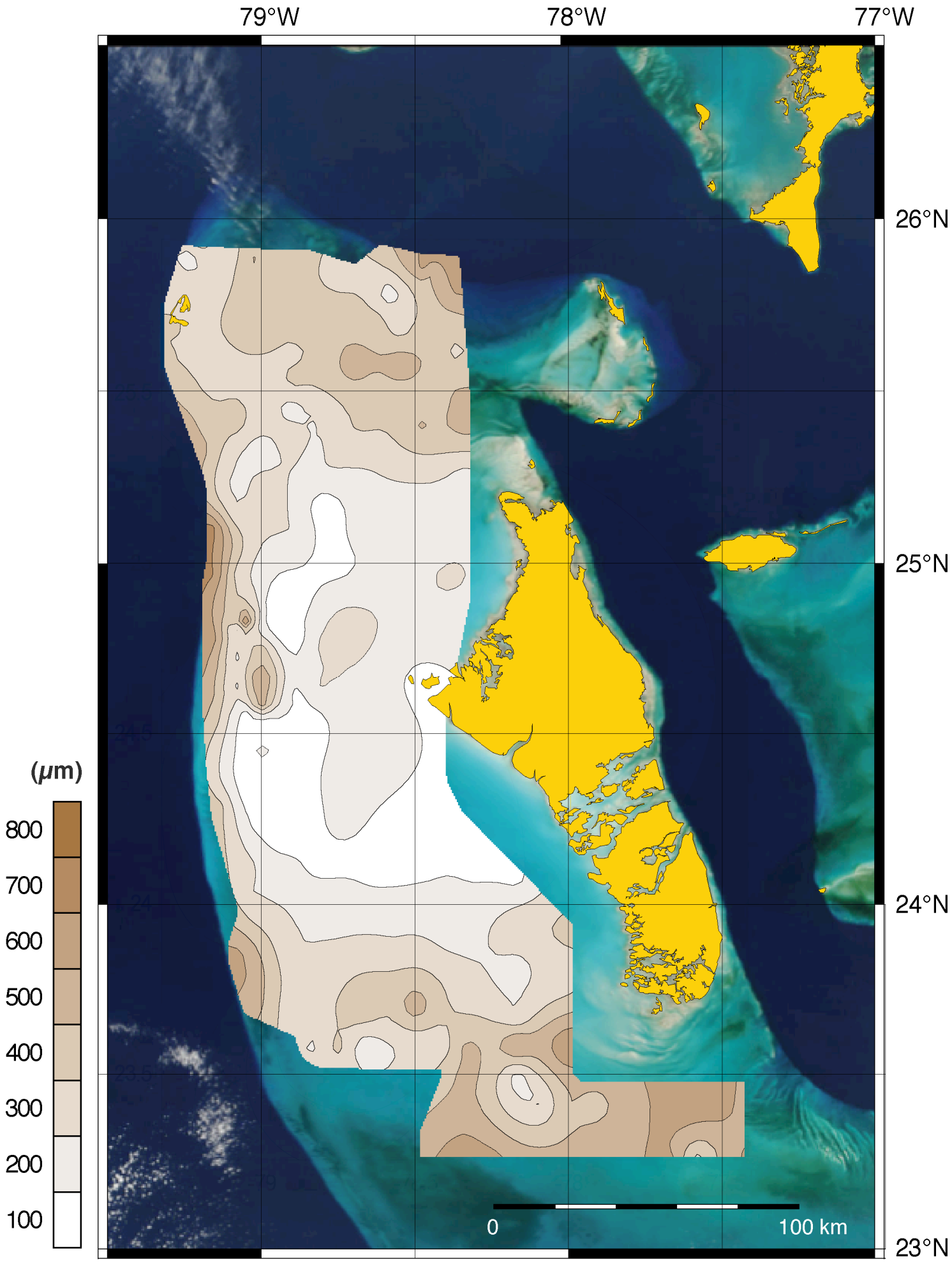

Reijmer et al.
Fig. 3A. Mean grain-size.

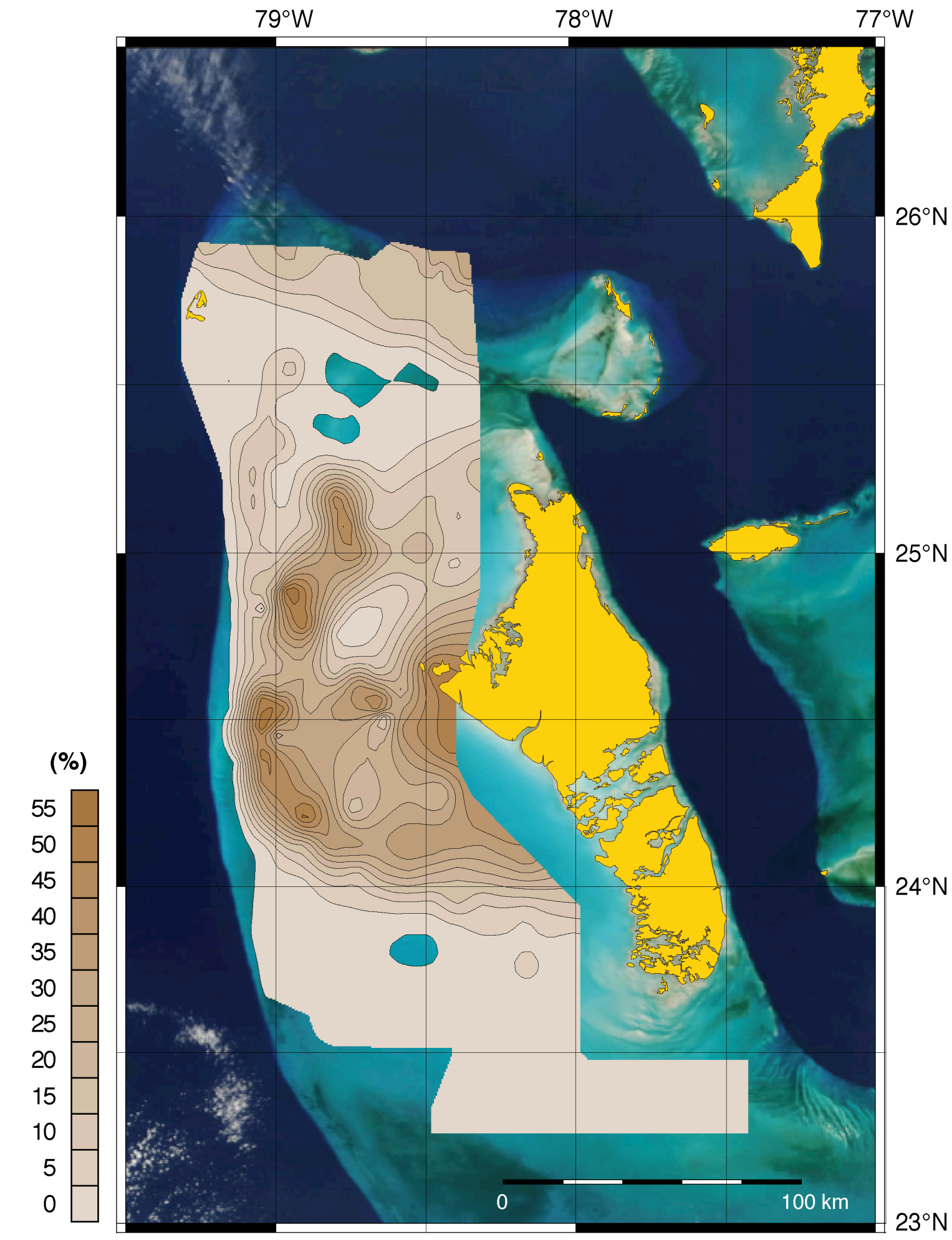

Reijmer et al.
Fig. 3B. Grain-size <63µm.

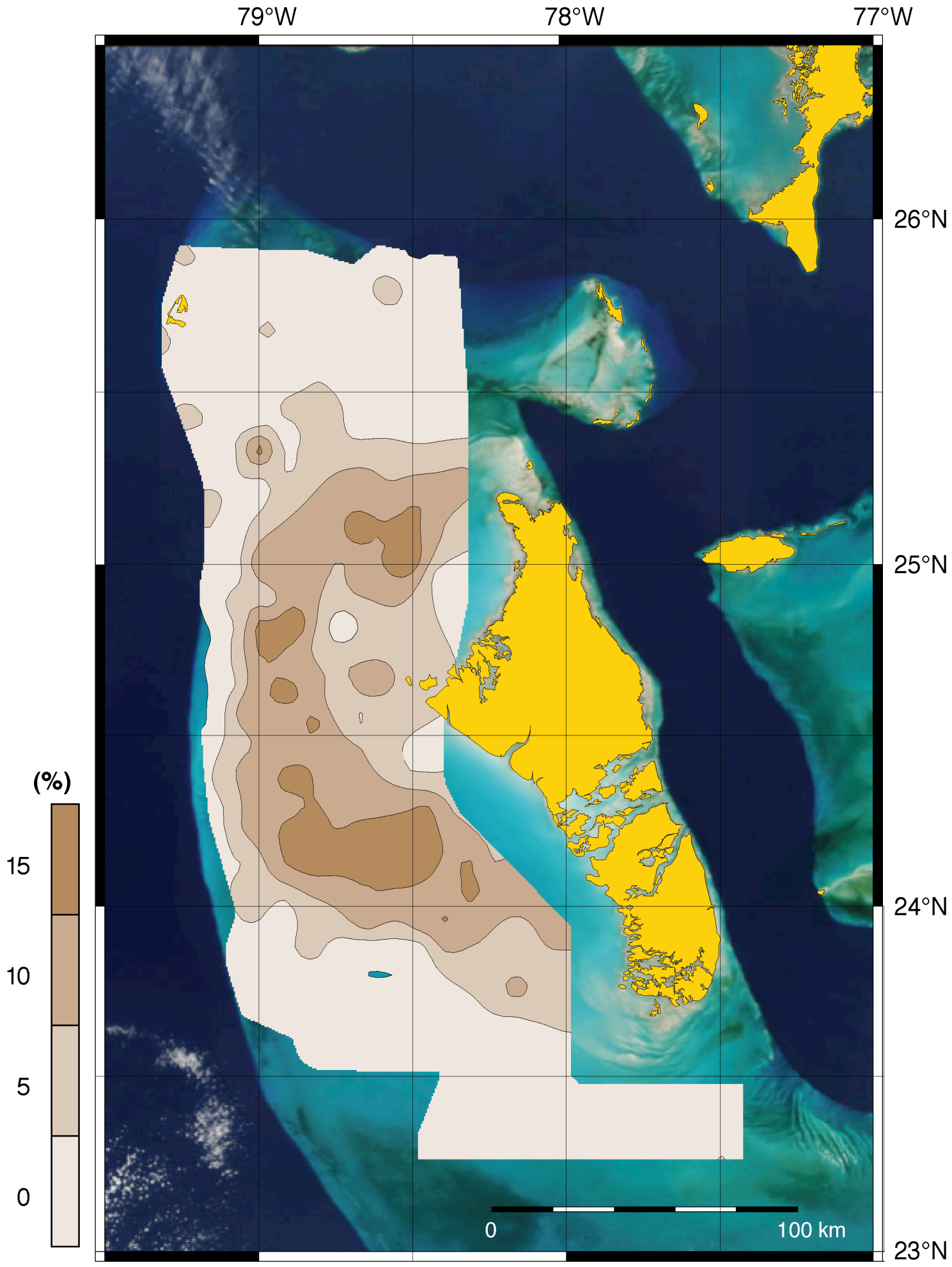

Reijmer et al.
Fig. 3C. Grain-size 63-125µm.

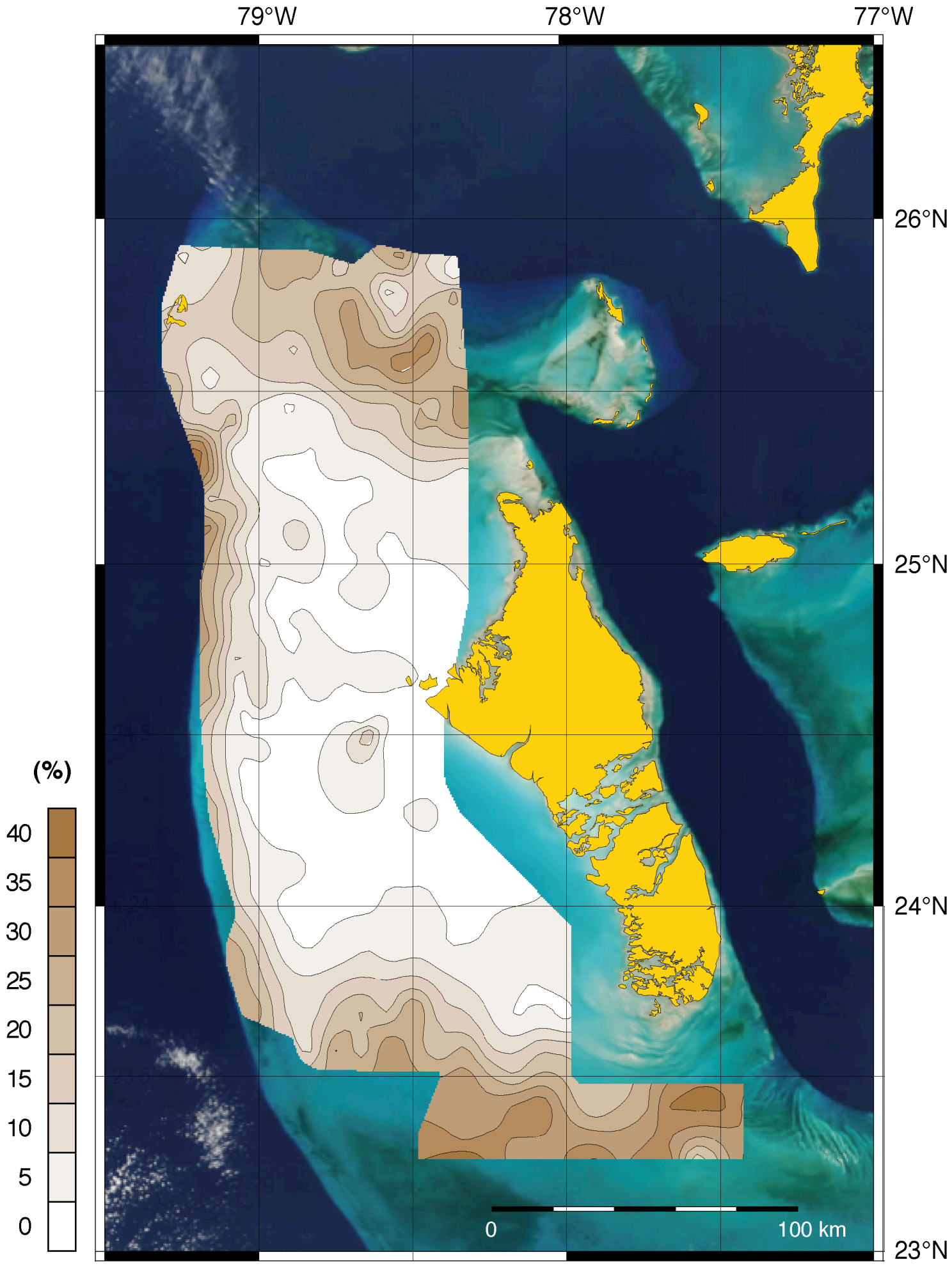

Reijmer et al.
Fig. 3D. Grain-size 500-1000µm.

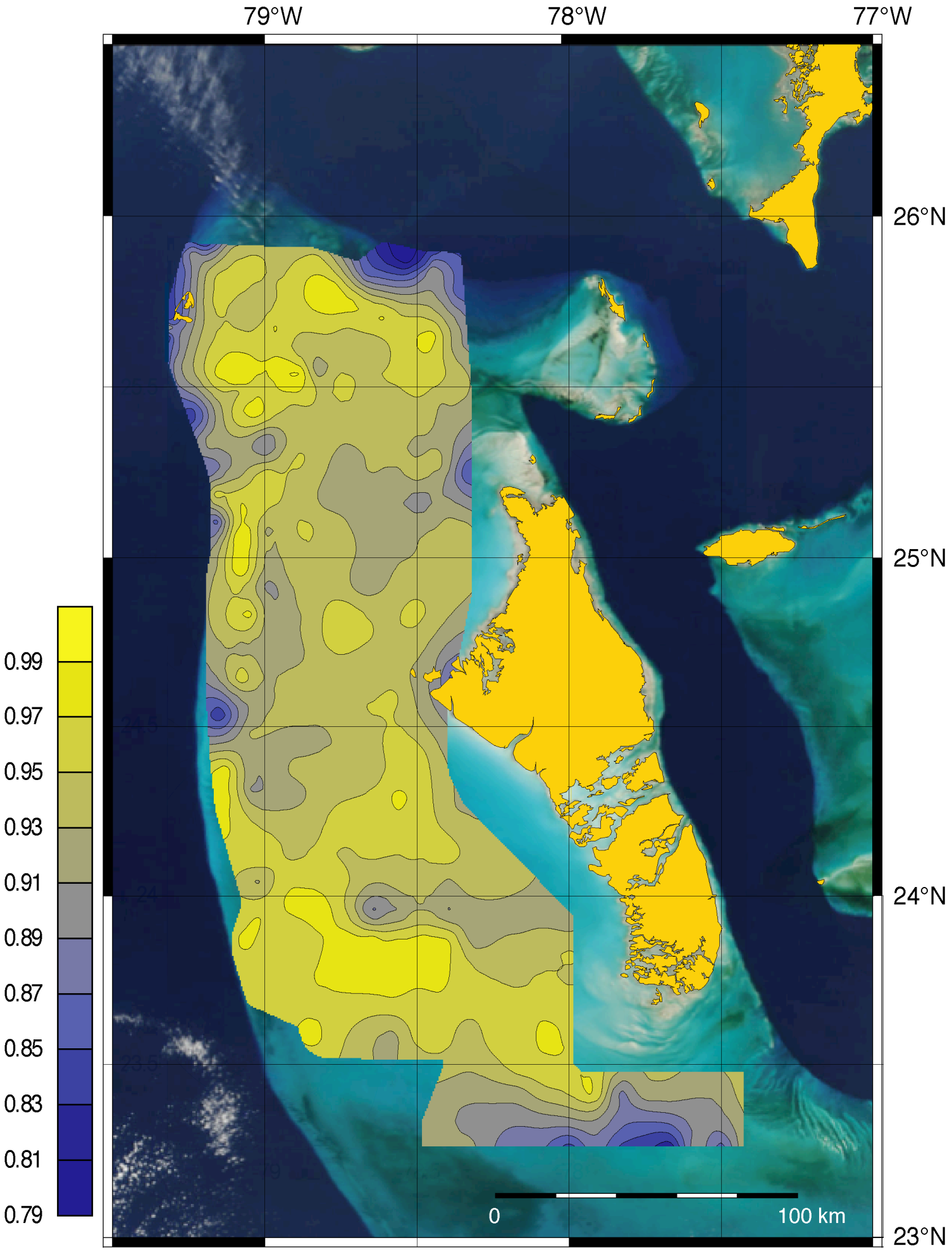

Reijmer et al.
Fig. 4A. Aragonite distribution (fractional abundance) .

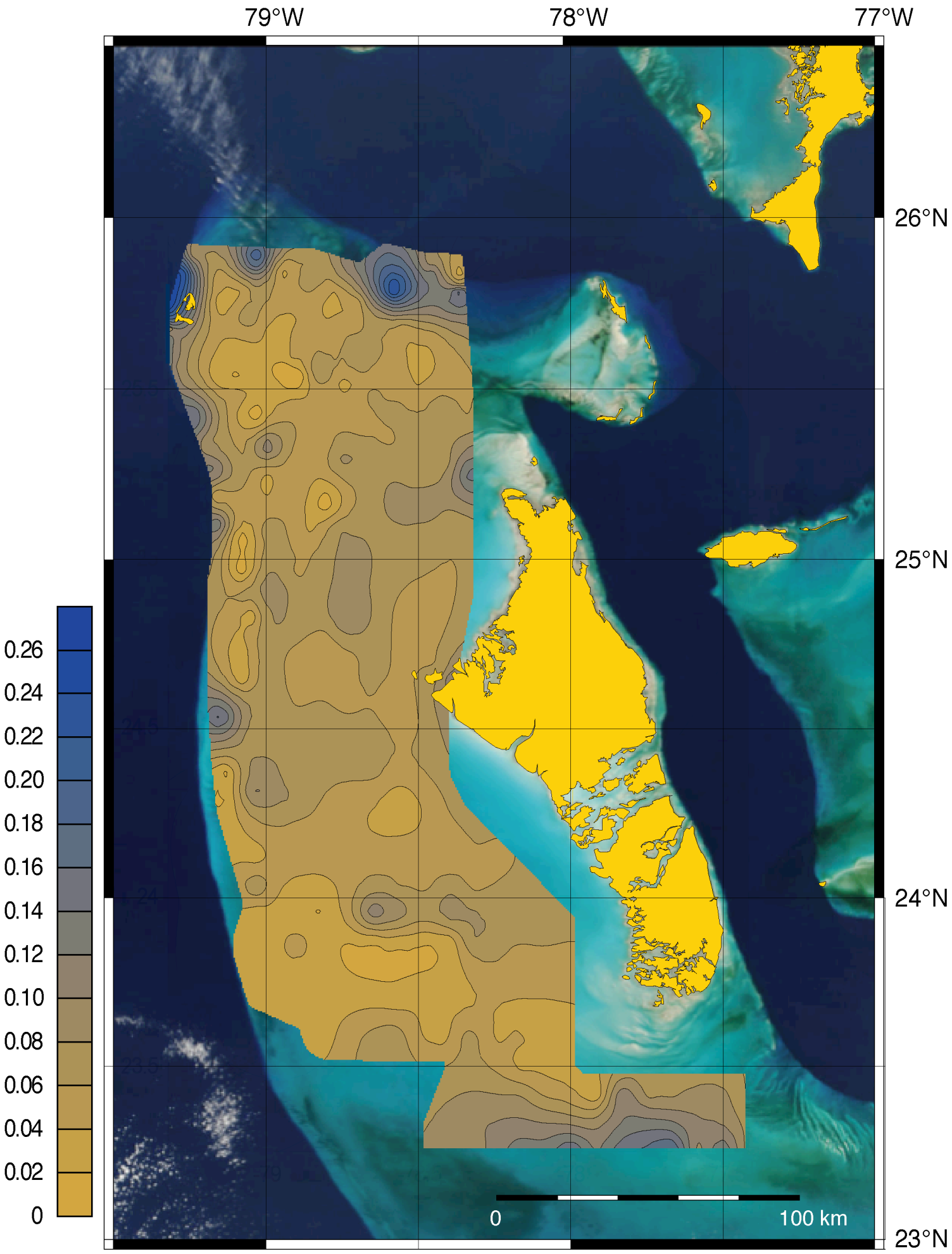

Reijmer et al.
Fig. 4B. High magnesium calcite distribution (fractional abundance) .

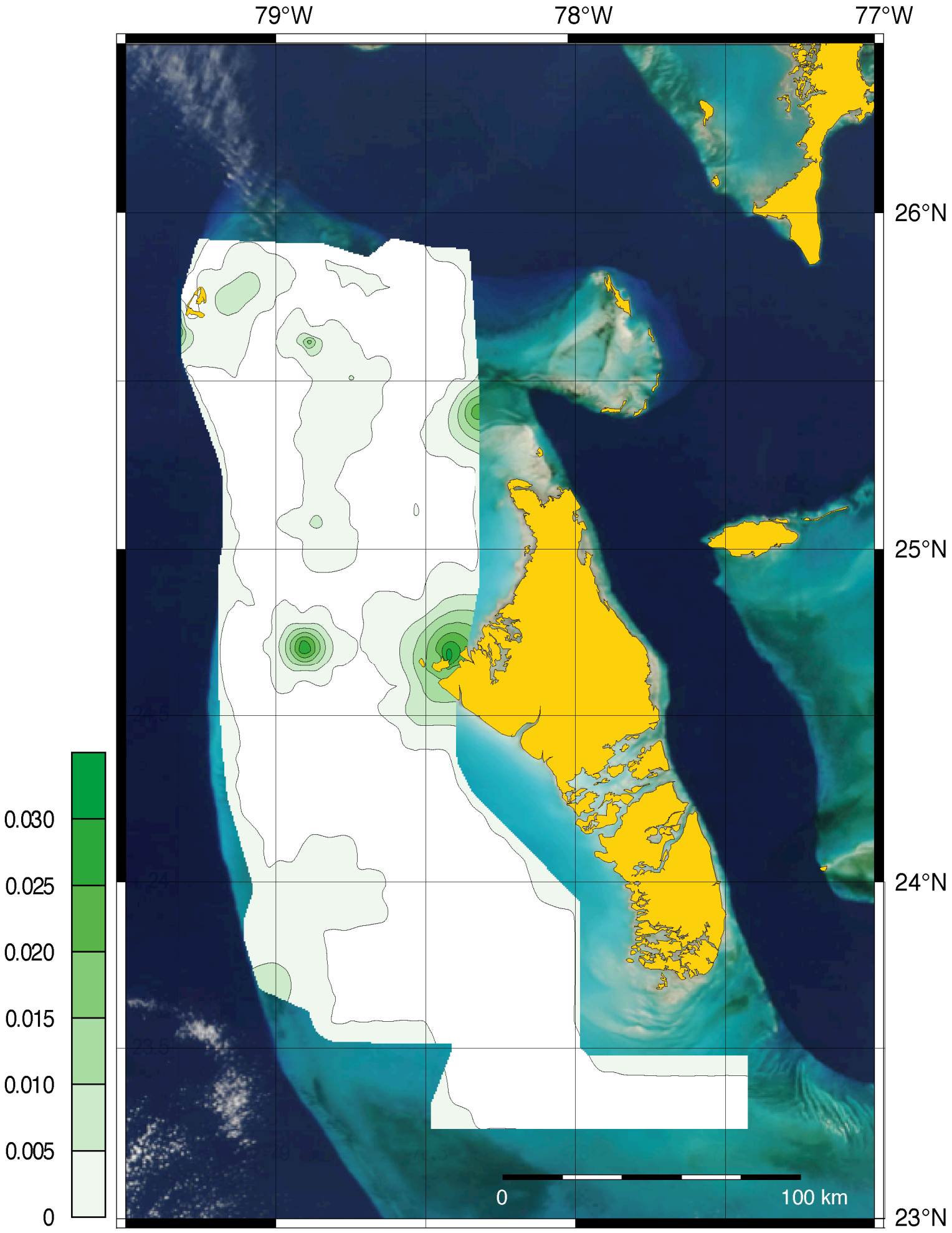

Reijmer et al.
Fig. 4C. Low magnesium calcite distribution (fractional abundance) .

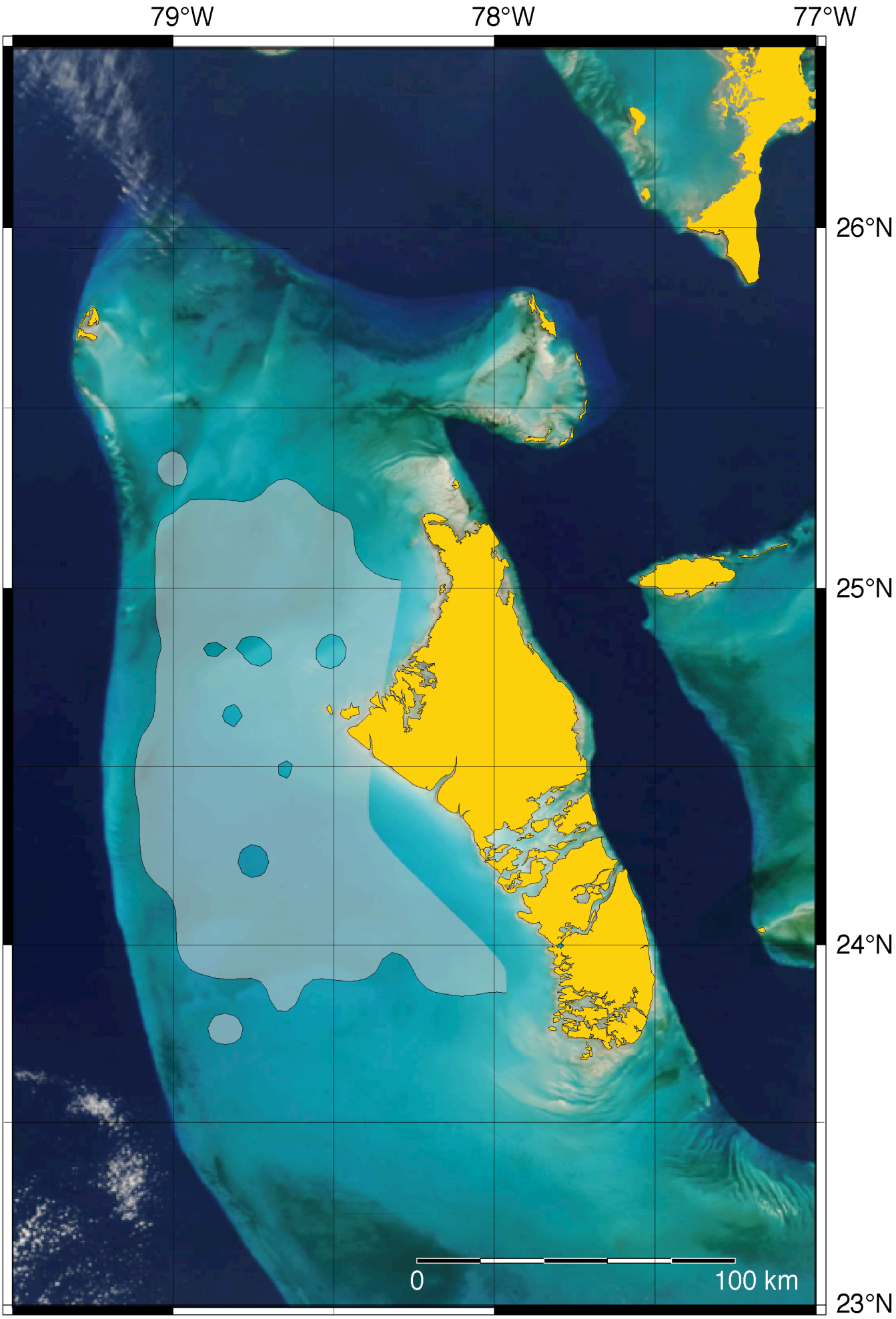

Reijmer et al.
Fig. 5A. Pellet distribution.

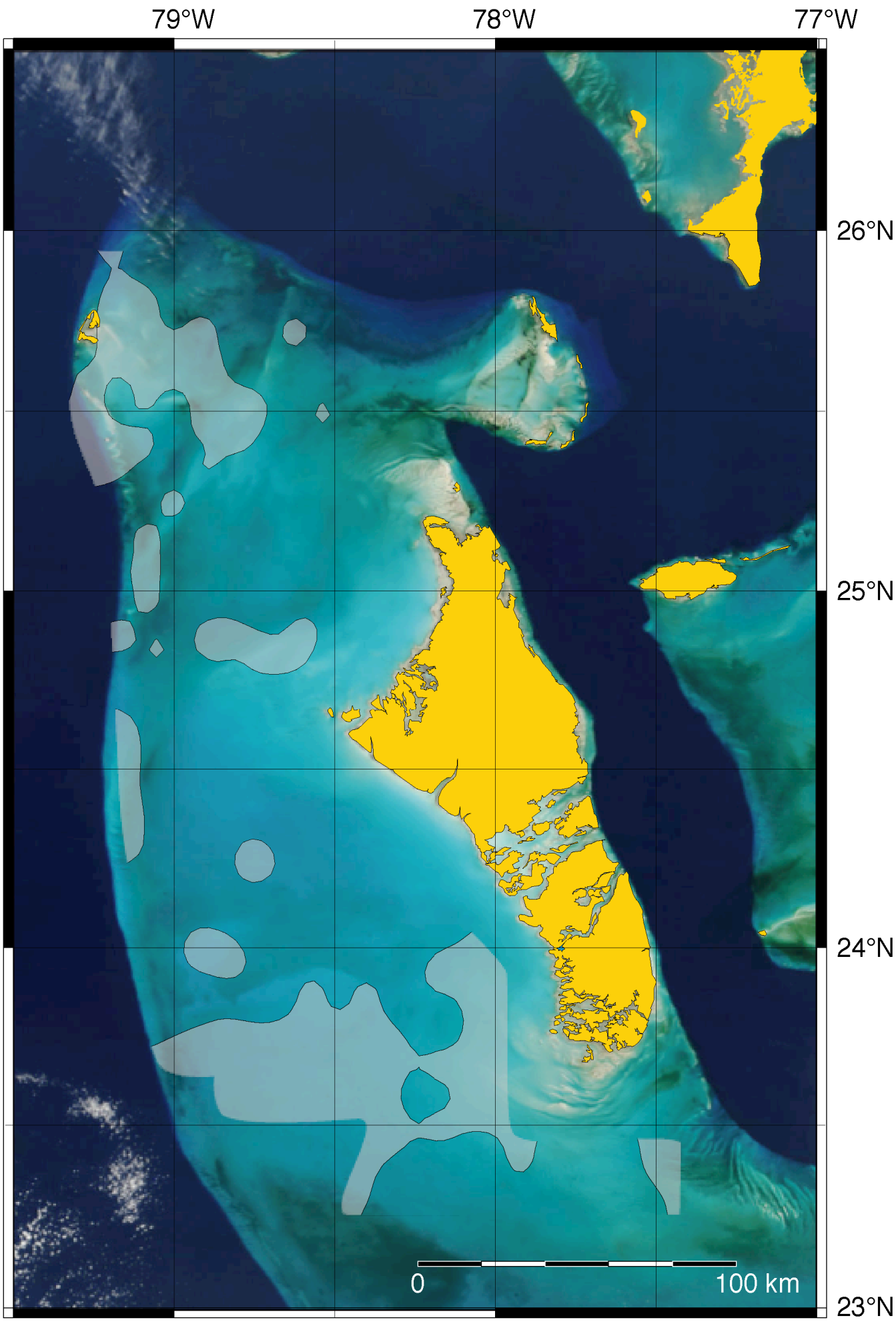

Reijmer et al.
Fig. 5B. Ooid distribution.

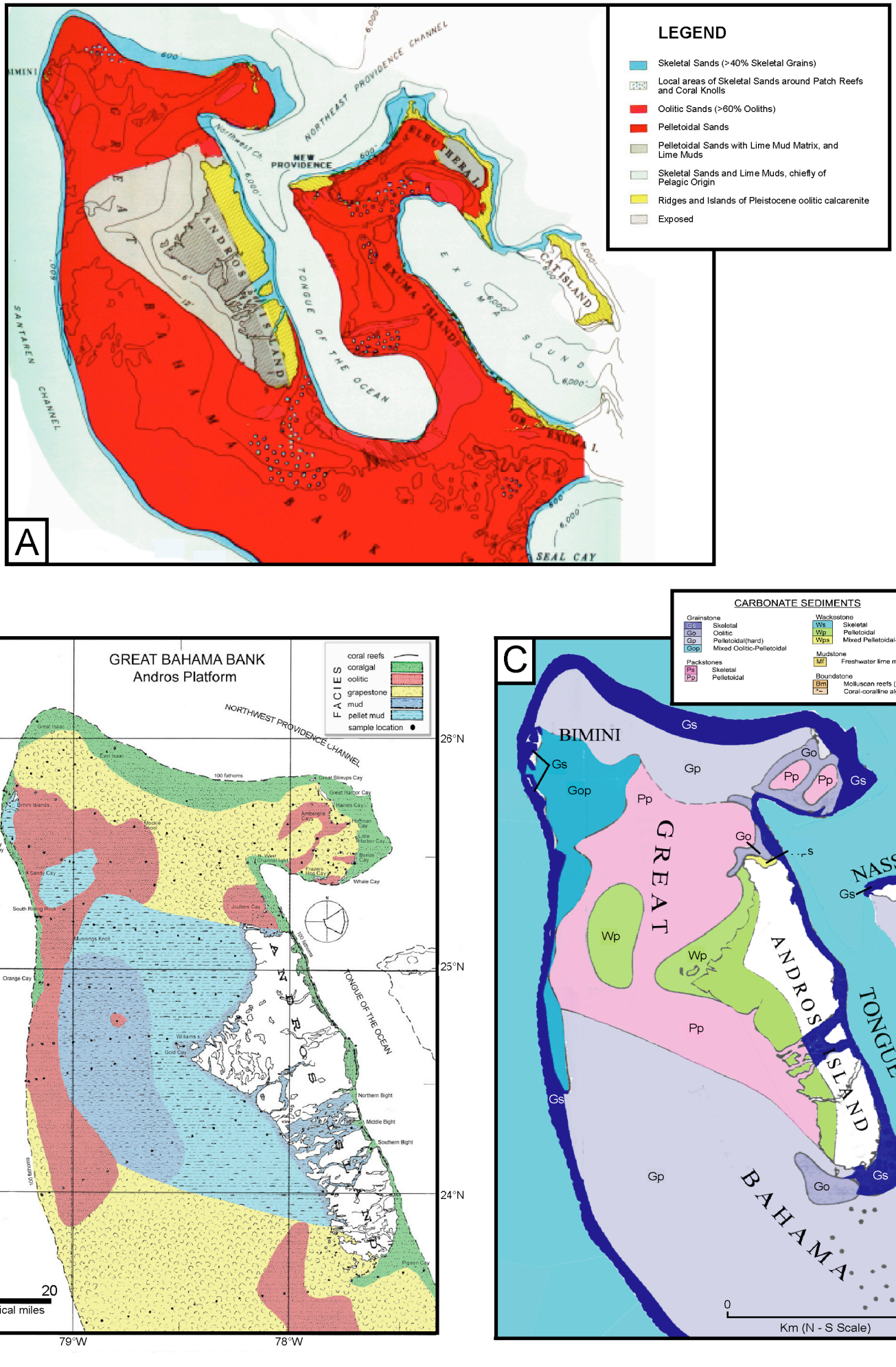

Reijmer et al.
Fig. 6. Facies maps.